Date: July 31, 2017
Title: Design of an Aperture Assembly for X-Ray Diffraction
Student: Christina Schmidt
Mentor: Dr. Peter Ko

Abstract:

Dr. Ko and I designed and built a new X-Ray diffraction aperture assembly which will be used at the Cornell High Energy Synchrotron Source (CHESS) F2 station. The F2 station is a dedicated high-energy facility (40-80 KeV) at CHESS with diverse user groups, ranging from research groups in engineering – who need to study stress, strain, fatigue and crack formation – to chemists and materials scientists, needing to learn more about novel energy materials comprising catalysts, batteries, and fuel cells. This assembly consists of a helium flight path (i.e. tubing), a metal disk with multiple holes with various radii (i.e. apertures), and mechanical stages for alignment. The assembly will be tested in the near future when X-rays become available for experiments.

Introduction:

In a typical synchrotron X-ray diffraction beamline, the size of the X-ray beam is defined using a set of slits (beam-defining slits) which is placed about one meter from the sample. Another set of slits (guard slits) is placed between the beam-defining slits and the sample to prevent scattered X-rays (by slits) from reaching the sample and detector. Due to divergence of synchrotron X-rays, the size of the incident beam on the sample is slightly larger than the opening of the slits (Als-Nielsen, Jens and Des McMorrow). Please refer to Figure 1 for a diagram of the layout at the F2 station.

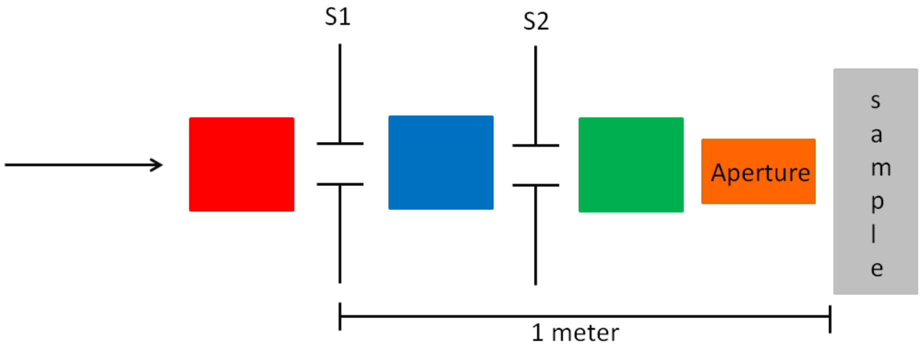

Figure 1: Schematic of the layout at F2. The arrow indicates the direction of X-rays. Red, blue, and green boxes are flux monitors (ion chambers). S1 and S2 are beam-defining and guard slits, respectively.

For certain experiments, someone may want to have better control over the size of the incident beam. This can be achieved by placing apertures, which only allow a portion of the X-rays from entering into a space, much closer (<10 millimeters) from the sample. When designing an aperture, the designer should consider what material it should be made out of and at what thickness. In addition, carefully consider for how to align the aperture must be made. As in many initial engineering designs, the first design iteration is rarely the final version.

<u>Design</u>:
The F2 station at CHESS uses energies between 40 and 80 KeV. The material of the aperture needs to sufficiently attenuate (needs to reduce the intensity of the beam) 40 to 80 KeV X-rays. The materials that were researched were tantalum, tungsten, and lead. The optimal thickness of the aperture at a variety of different energies was determined using Beer's law, $\frac{I}{I_0} = e^{-\mu * t}$ (Hubbell, J.H. and S. M Seltzer). I_0 is the initial intensity of the incoming X-rays and I is the transmitted intensity (after the X-rays have traveled through a material with thickness), t, and μ, absorption coefficients, (which depends on atomic or molecular weight of the material and the material's density). Absorption coefficients of various materials can be found in reference tables (Hubbell, J. H. and Seltzer, J. M.). Figure 2 shows thicknesses of tantalum, tungsten and lead which will result in $I/I_0=10^{-10}$. See Appendix Table 1 for the tabulated values.

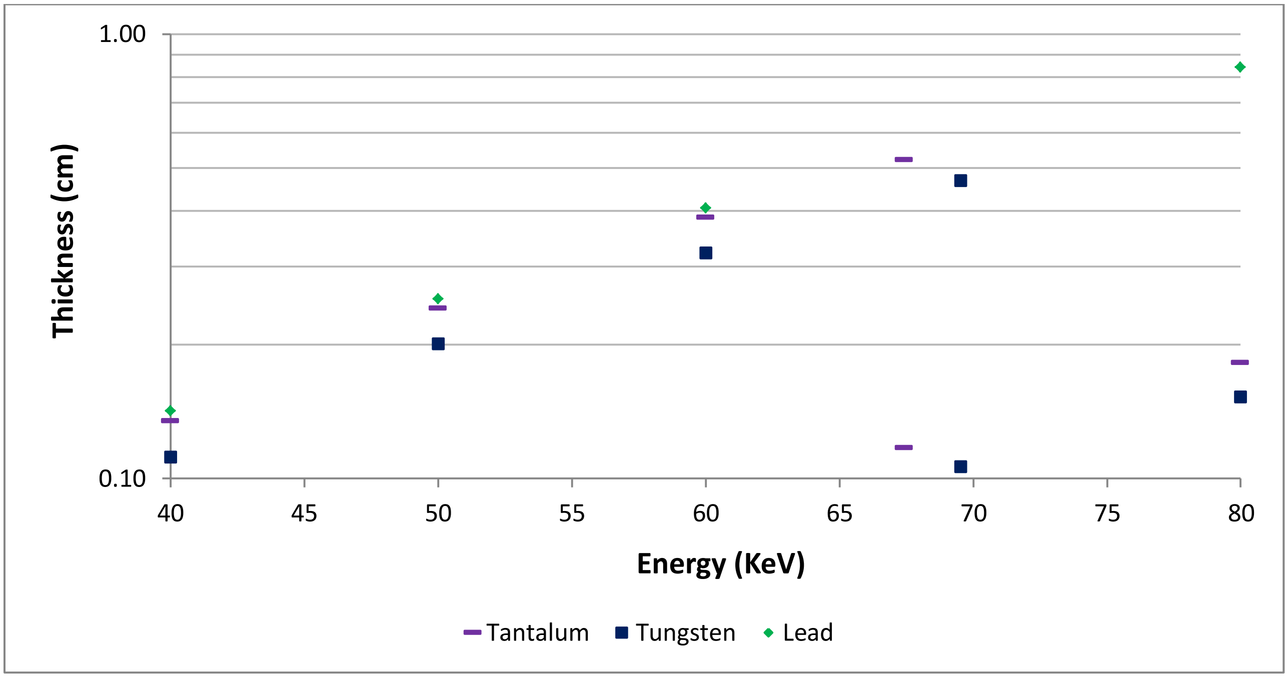

Figure 2: Thickness of tantalum, tungsten and lead that will yield $I/I_0=10^{-10}$ at energies from 40 to 80 KeV

The thickness that will be used will be at 60 KeV because 60 KeV is the most commonly used energy level at the F2 station. The thickness at 60 KeV was used to find the intensity for the same energy levels from above. The graph in Figure 3 shows I/I_0 between 40 and 80 KeV with tantalum, tungsten and lead with thickness equal to 0.32 cm, 0.39 cm and 0.41 cm, respectively. See Appendix Table 2 for the tabulated values. Both Figure 2 and Figure 3 shows that generally the higher the energy, the more the x-rays can move through the material. Note the sudden drop in thickness or I/I_0 for tantalum and tungsten between 65 and 70 KeV is due to the absorption edges of the two metals (tantalum at 67.416 KeV, tungsten at 69.525 KeV).

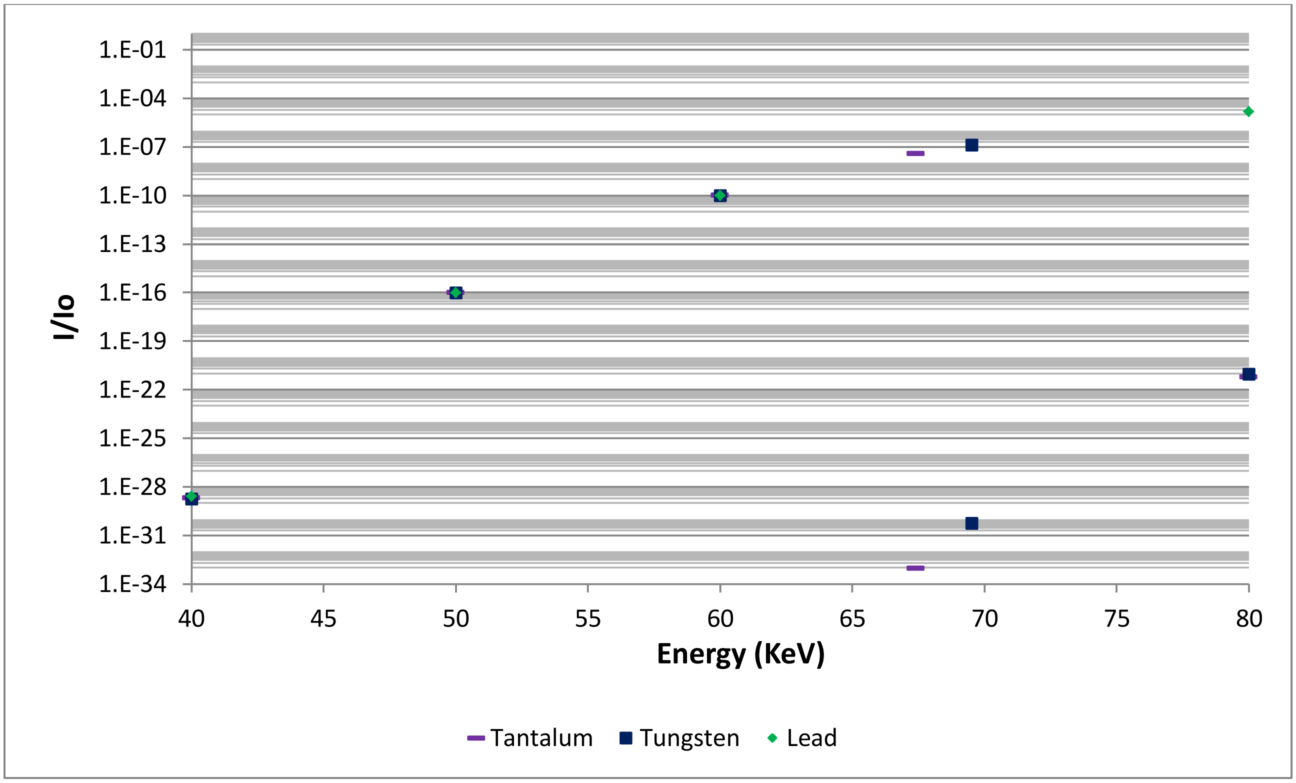

Figure 3: I/I_0 vs energy at a constant thickness. Thicknesses of tantalum, tungsten, and lead are 0.32 cm, 0.39 cm and 0.41 cm, respectively.

After careful consideration, the material for the aperture was determined to be “heavy-met”. “Heavy-met” contains mostly tungsten and some lighter metals. Tungsten and tantalum are very hard materials and it would be difficult to work with them. Machining lead poses long term health risks. Thus, “heavy met” is a good material to use.

The design for this aperture assembly will be different than the typical aperture. It consists of tubing, which acts as a flight path and a 3 millimeter-thick heavy-met disk with multiple holes with varying radii at one end of the tubing. The aperture will be located in the tube that is the closest to the sample. The X-rays will travel through the tubing and then they will go through the aperture before interacting with the sample. The tubing will have helium gas inside because “light” gases decreases the X-rays scattering relative to travel in air. To prevent the gas from escaping the tube, both ends will be sealed with Kapton® (polyimide) tape, which is transparent to X-rays, and functions as a window material. A view of the designed tubing can be found in Figure 4. Not shown in the picture are gas inline shut-off couplers (Grainger, 2YCW7), which are threaded to the holes on the tubing wall.

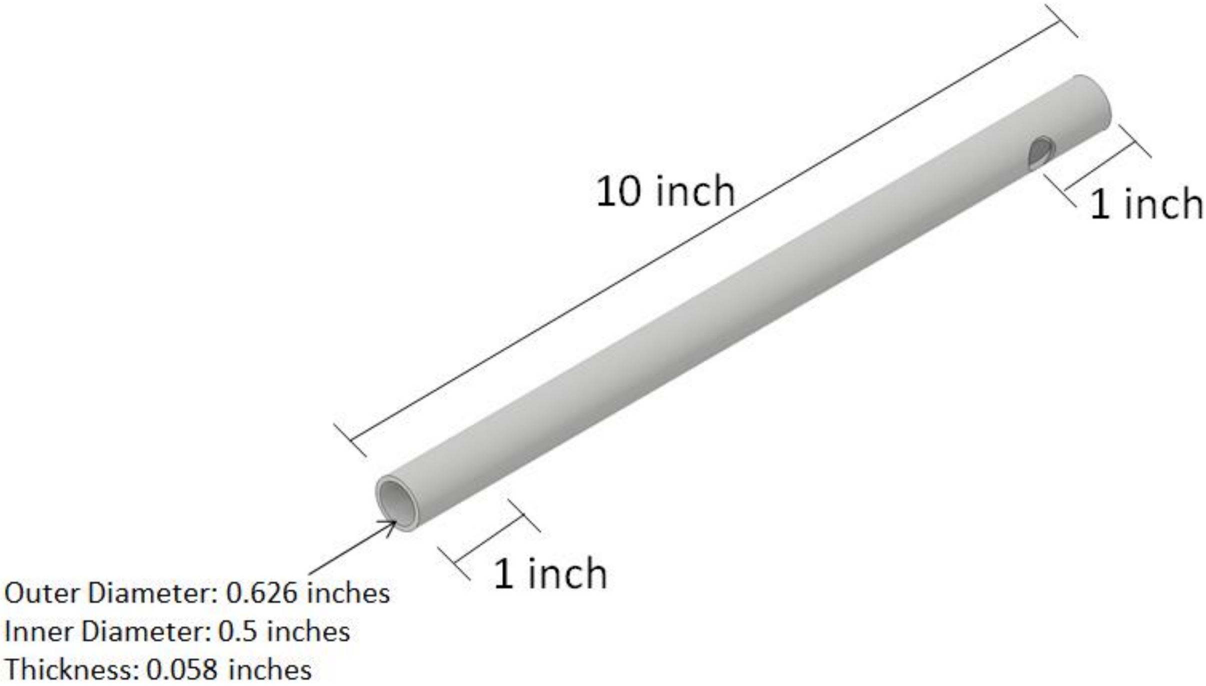

Figure 4: CAD drawing of the aperture tubing. See Appendix Figure 1 for detailed drawings.

One criterion my mentor and I had for this project was to increase productivity for the users. It was decided that the aperture will have multiple holes that are aligned along the center line. The holes will slightly decrease in size as you move down the diameter. These holes diameters will be equally spaced and between the sizes of 1.5 millimeter and 0.5 millimeter. This will allow about four to five millimeters to be the minimal distance from the end of the hole to the edge of the tube. We decided to make the aperture holes slightly tapered, about one degree. This prevents small-angle scattering of the aperture openings from travelling further – this is equivalent to having a set of guard slits downstream of beam-defining slits. Scattering increases when the roughness of the holes edges increase. The chances of a machinist drilling a precise straight hole decreases as the diameter decreases. A view of the aperture can be found in Figure 5.

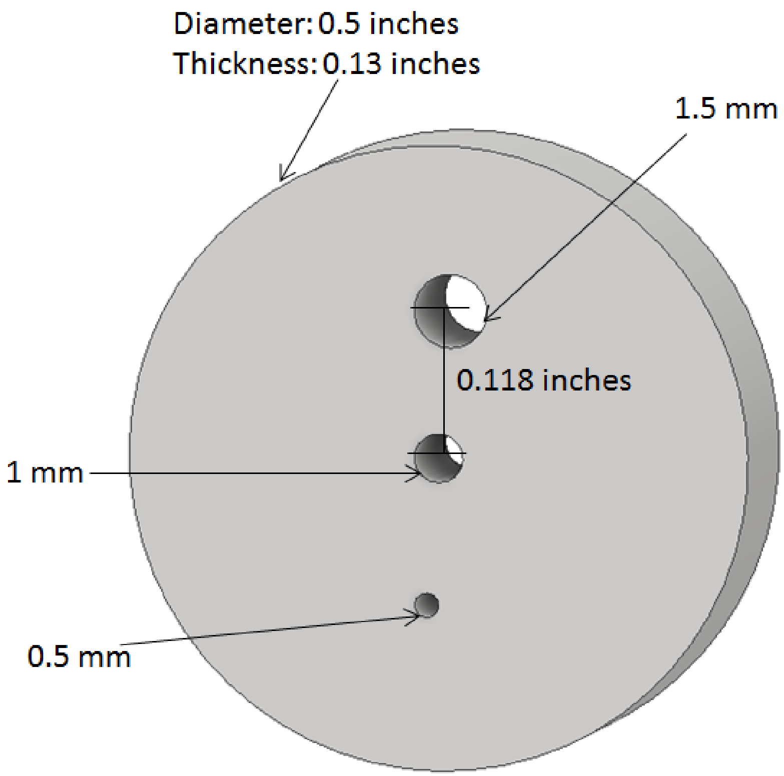

Figure 5: CAD drawing of the aperture. See Appendix Figure 2 for detailed drawings.

The aperture cannot stand on its own. There is a need for an apparatus that can hold the tube. It was planned that the tube will be in a V-clamp holder (Thorlabs, VC3C). A picture of the V-clamp holder is below in Figure 6.

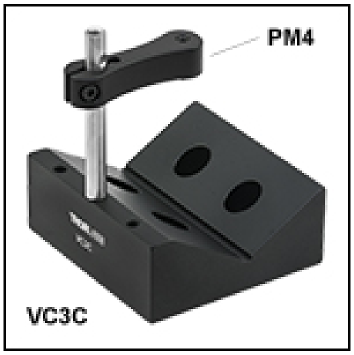

Figure 6: This is a picture of the V-clamp that is used in the aperture assembly (Thorlabs)

This holder has four 1.5 inch legs (Thorlabs, TR1.5) which are attached to a plate and then to rotation and translation stages (Huber, Goniometer 408). The stages allow the user to mechanically control all necessary motions for alignment of the tube from outside the experiment station. To mate the V-clamp holder with legs to the rotation stage, we designed a plate, which is shown in Figure 7.

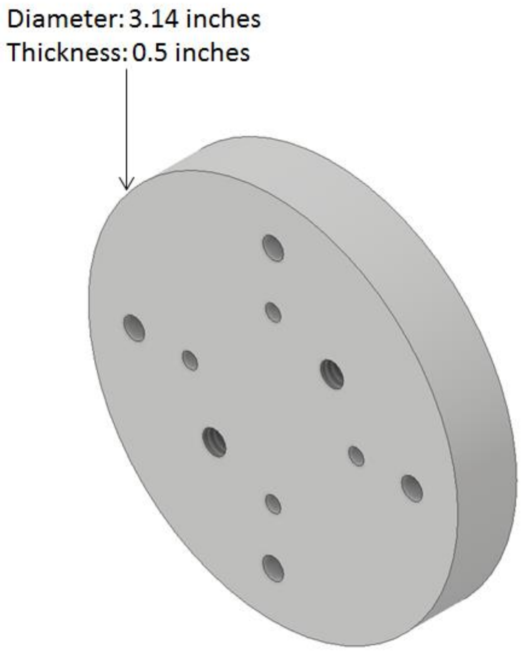

Figure 7: CAD drawing of the mating plate. See Appendix Figure 3 for detailed drawings.

<u>Future Plans</u>:
We still need to test the tube with gas to make sure it does not leak. Also, we have to test the product with all parts assembled in the F2 station. We would like to do additional testing when the prototype assembly is complete. After the testing is complete, we will be able to make a conclusion and possibly a revision. A view of the aperture assembly is found in Figure 8.

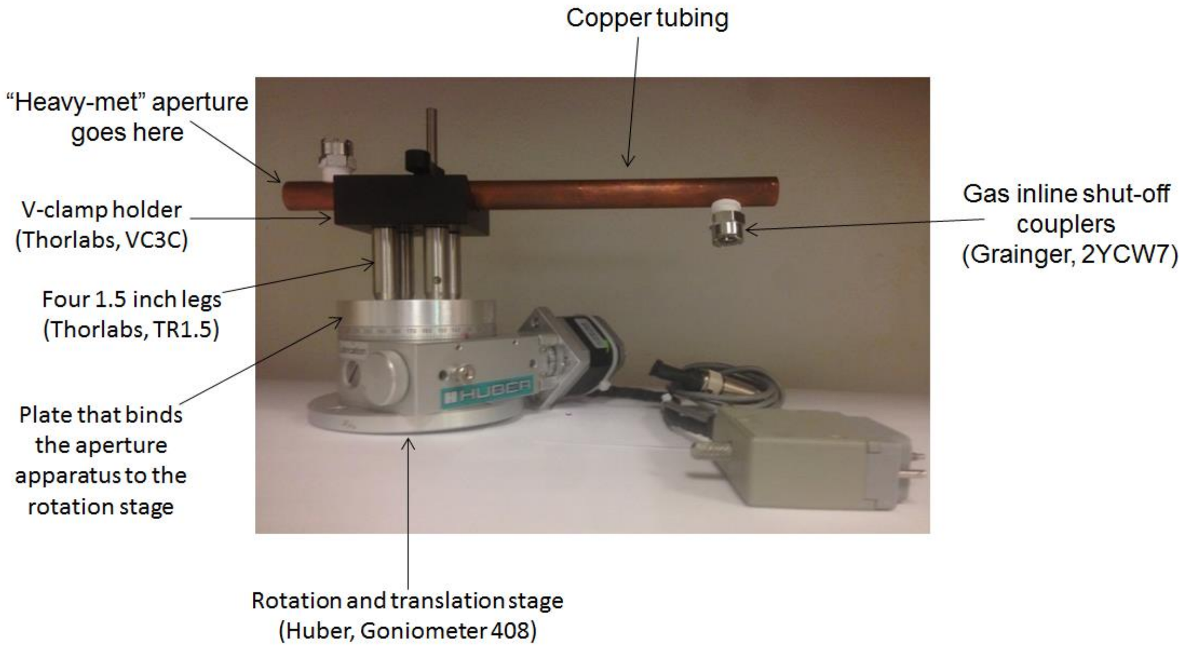

Figure 8: The aperture assembly

References:

1. Als-Nielsen, Jens, and Des McMorrow. (2011). *Elements of Modern X-ray Physics*. John Wiley & Sons, Ltd.
2. Hubbell, J.H. and S. M Seltzer. (1996). X-Ray Mass Attenuation Coefficients: Tables of X-Ray Mass Energy-Absorption Coefficients from 1 KeV to 20 MeV for elements Z = 1 to 92 and 48 Additional Substances of Dosimetric Interest. NIST Physical Measurement Laboratory, retrieved from https://www.nist.gov/pml/x-ray-mass-attenuation-coefficients.
3. Thompson, Albert C. *et al.*, (2009). *X-ray Data Booklet*. Lawrence Berkeley National Laboratory, University of California, Berkeley CA, retrieved from http://xdb.lbl.gov/

Acknowledgments:

Participating in the Summer Research for Community College Students (SRCCS) at Cornell University has been an incredible and tremendously rewarding learning experience. This SRCCS internship has helped me explore the field of engineering, with a supporting mentor, and to solve real technical challenges in a much more profound and insightful way rather than in a typical class room environment.

I would like to thank everyone that I worked with this summer at Cornell. Some of the people in particular that were very helpful were Peter Ko, Carl Franck, Ken Finkelstein, Christopher Budrow, Jerry Houghton, Stephan Felix, and Lora Hine. I greatly appreciate their time, guidance, patience, and all the helpful advice they shared with me this summer.

This work was performed at CHESS which is supported by the National Science Foundation under NSF award DMR-1332208. I would like to acknowledge the grant from the National Science Foundation for providing financial support for SRCCS interns at Cornell University.

Appendix:

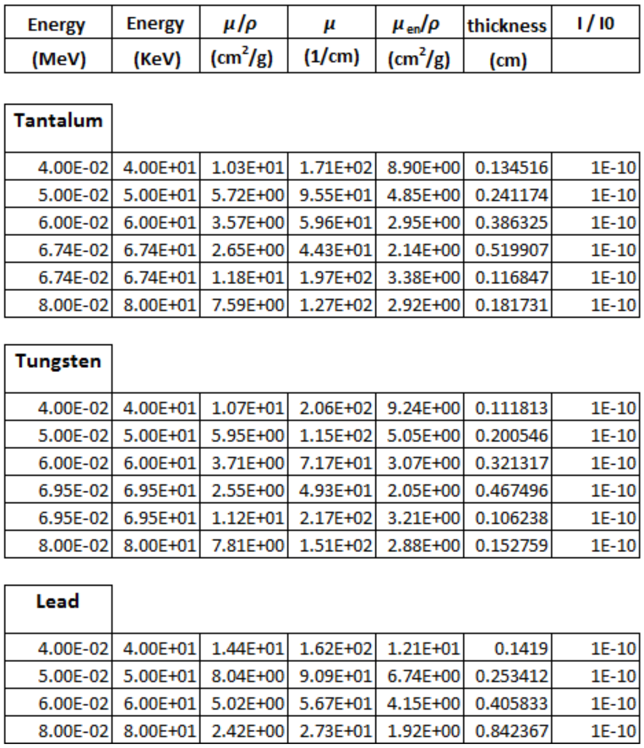

Energy	Energy	μ/ρ	μ	μ_{en}/ρ	thickness	I / I0
(MeV)	(KeV)	(cm^2/g)	(1/cm)	(cm^2/g)	(cm)	
Tantalum						
4.00E-02	4.00E+01	1.03E+01	1.71E+02	8.90E+00	0.134516	1E-10
5.00E-02	5.00E+01	5.72E+00	9.55E+01	4.85E+00	0.241174	1E-10
6.00E-02	6.00E+01	3.57E+00	5.96E+01	2.95E+00	0.386325	1E-10
6.74E-02	6.74E+01	2.65E+00	4.43E+01	2.14E+00	0.519907	1E-10
6.74E-02	6.74E+01	1.18E+01	1.97E+02	3.38E+00	0.116847	1E-10
8.00E-02	8.00E+01	7.59E+00	1.27E+02	2.92E+00	0.181731	1E-10
Tungsten						
4.00E-02	4.00E+01	1.07E+01	2.06E+02	9.24E+00	0.111813	1E-10
5.00E-02	5.00E+01	5.95E+00	1.15E+02	5.05E+00	0.200546	1E-10
6.00E-02	6.00E+01	3.71E+00	7.17E+01	3.07E+00	0.321317	1E-10
6.95E-02	6.95E+01	2.55E+00	4.93E+01	2.05E+00	0.467496	1E-10
6.95E-02	6.95E+01	1.12E+01	2.17E+02	3.21E+00	0.106238	1E-10
8.00E-02	8.00E+01	7.81E+00	1.51E+02	2.88E+00	0.152759	1E-10
Lead						
4.00E-02	4.00E+01	1.44E+01	1.62E+02	1.21E+01	0.1419	1E-10
5.00E-02	5.00E+01	8.04E+00	9.09E+01	6.74E+00	0.253412	1E-10
6.00E-02	6.00E+01	5.02E+00	5.67E+01	4.15E+00	0.405833	1E-10
8.00E-02	8.00E+01	2.42E+00	2.73E+01	1.92E+00	0.842367	1E-10

Appendix Table 1: Tabulated Values for calculating thickness using Beer's law. Figure 2 shows plots of thickness vs energy for tantalum, tungsten, and lead.

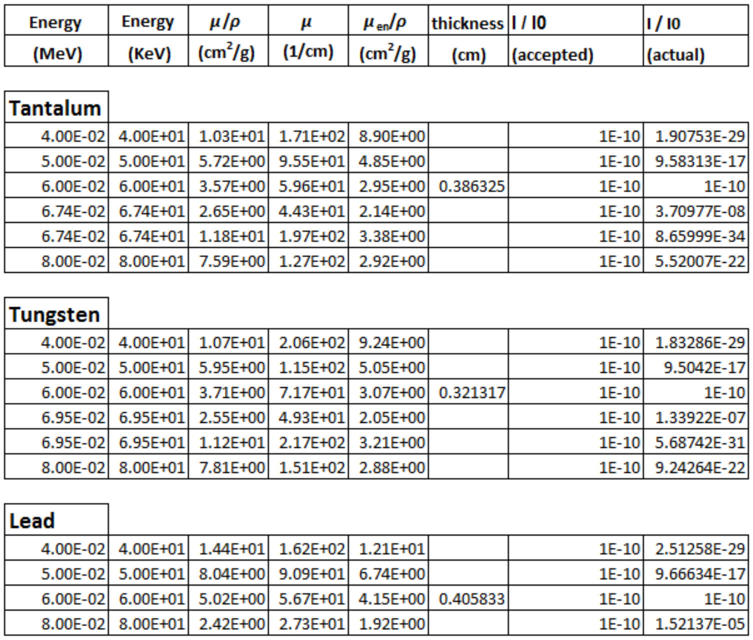

Energy	Energy	μ/ρ	μ	μ_{en}/ρ	thickness	I / I0	I / I0
(MeV)	(KeV)	(cm^2/g)	(1/cm)	(cm^2/g)	(cm)	(accepted)	(actual)
Tantalum							
4.00E-02	4.00E+01	1.03E+01	1.71E+02	8.90E+00		1E-10	1.90753E-29
5.00E-02	5.00E+01	5.72E+00	9.55E+01	4.85E+00		1E-10	9.58313E-17
6.00E-02	6.00E+01	3.57E+00	5.96E+01	2.95E+00	0.386325	1E-10	1E-10
6.74E-02	6.74E+01	2.65E+00	4.43E+01	2.14E+00		1E-10	3.70977E-08
6.74E-02	6.74E+01	1.18E+01	1.97E+02	3.38E+00		1E-10	8.65999E-34
8.00E-02	8.00E+01	7.59E+00	1.27E+02	2.92E+00		1E-10	5.52007E-22
Tungsten							
4.00E-02	4.00E+01	1.07E+01	2.06E+02	9.24E+00		1E-10	1.83286E-29
5.00E-02	5.00E+01	5.95E+00	1.15E+02	5.05E+00		1E-10	9.5042E-17
6.00E-02	6.00E+01	3.71E+00	7.17E+01	3.07E+00	0.321317	1E-10	1E-10
6.95E-02	6.95E+01	2.55E+00	4.93E+01	2.05E+00		1E-10	1.33922E-07
6.95E-02	6.95E+01	1.12E+01	2.17E+02	3.21E+00		1E-10	5.68742E-31
8.00E-02	8.00E+01	7.81E+00	1.51E+02	2.88E+00		1E-10	9.24264E-22
Lead							
4.00E-02	4.00E+01	1.44E+01	1.62E+02	1.21E+01		1E-10	2.51258E-29
5.00E-02	5.00E+01	8.04E+00	9.09E+01	6.74E+00		1E-10	9.66634E-17
6.00E-02	6.00E+01	5.02E+00	5.67E+01	4.15E+00	0.405833	1E-10	1E-10
8.00E-02	8.00E+01	2.42E+00	2.73E+01	1.92E+00		1E-10	1.52137E-05

Appendix Table 2: Tabulated values for calculating I/I_0 using constant thickness of tantalum, tungsten and lead. Figure 3 shows plots of I/I_0 vs energy for tantalum, tungsten and lead.

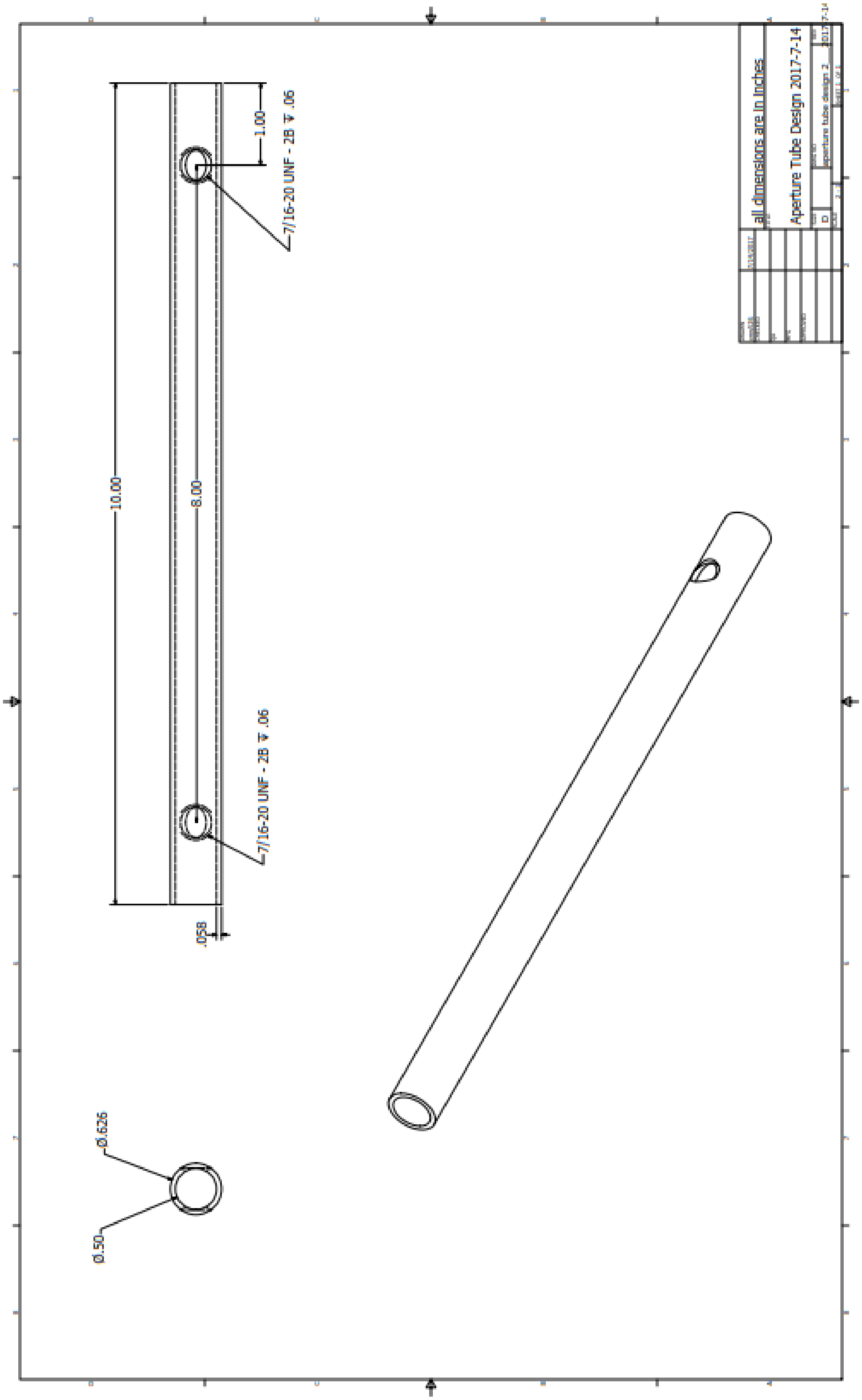

Appendix Figure 1: Detailed drawings of the tubing

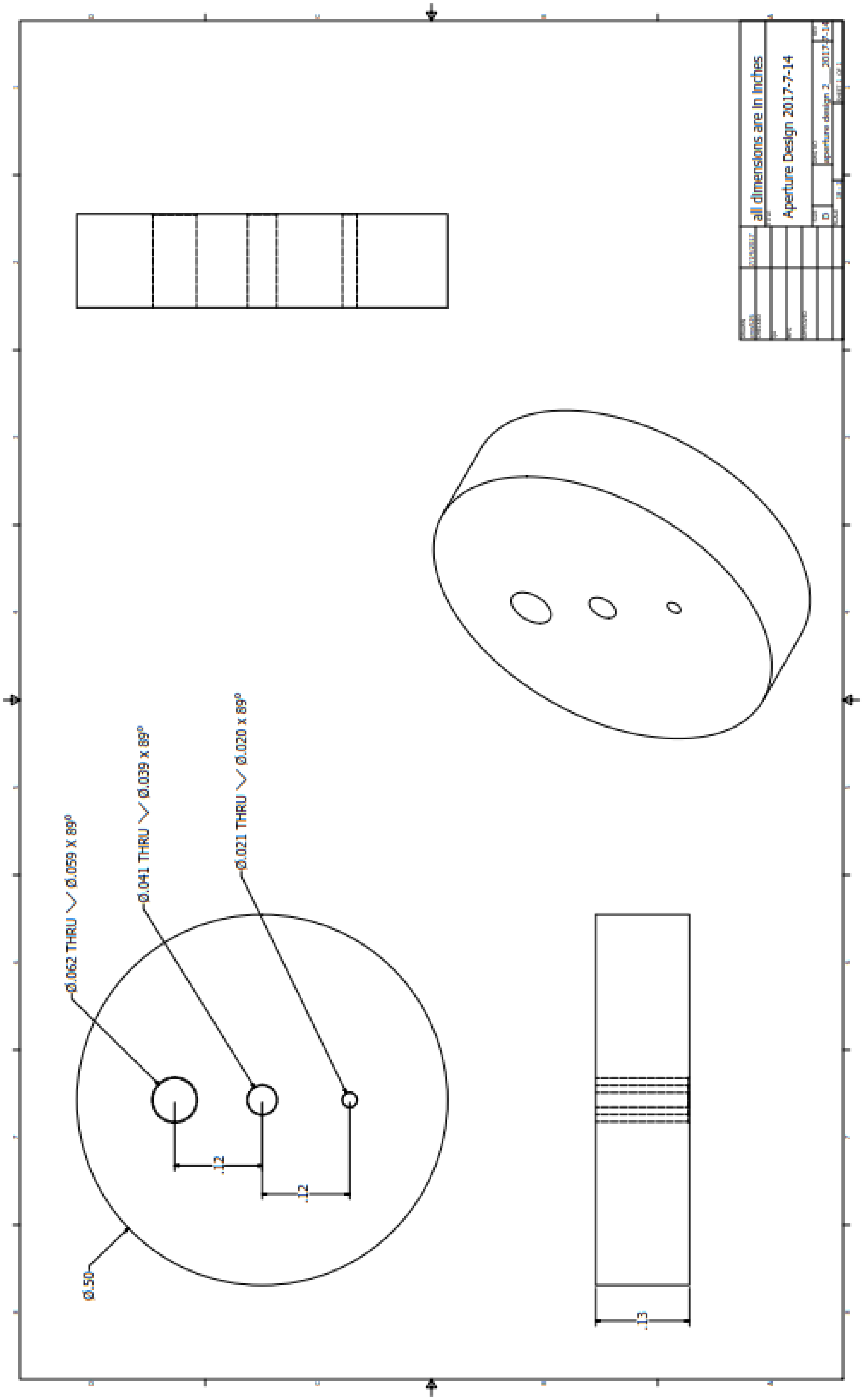

Appendix Figure 2: Detailed drawings of the aperture

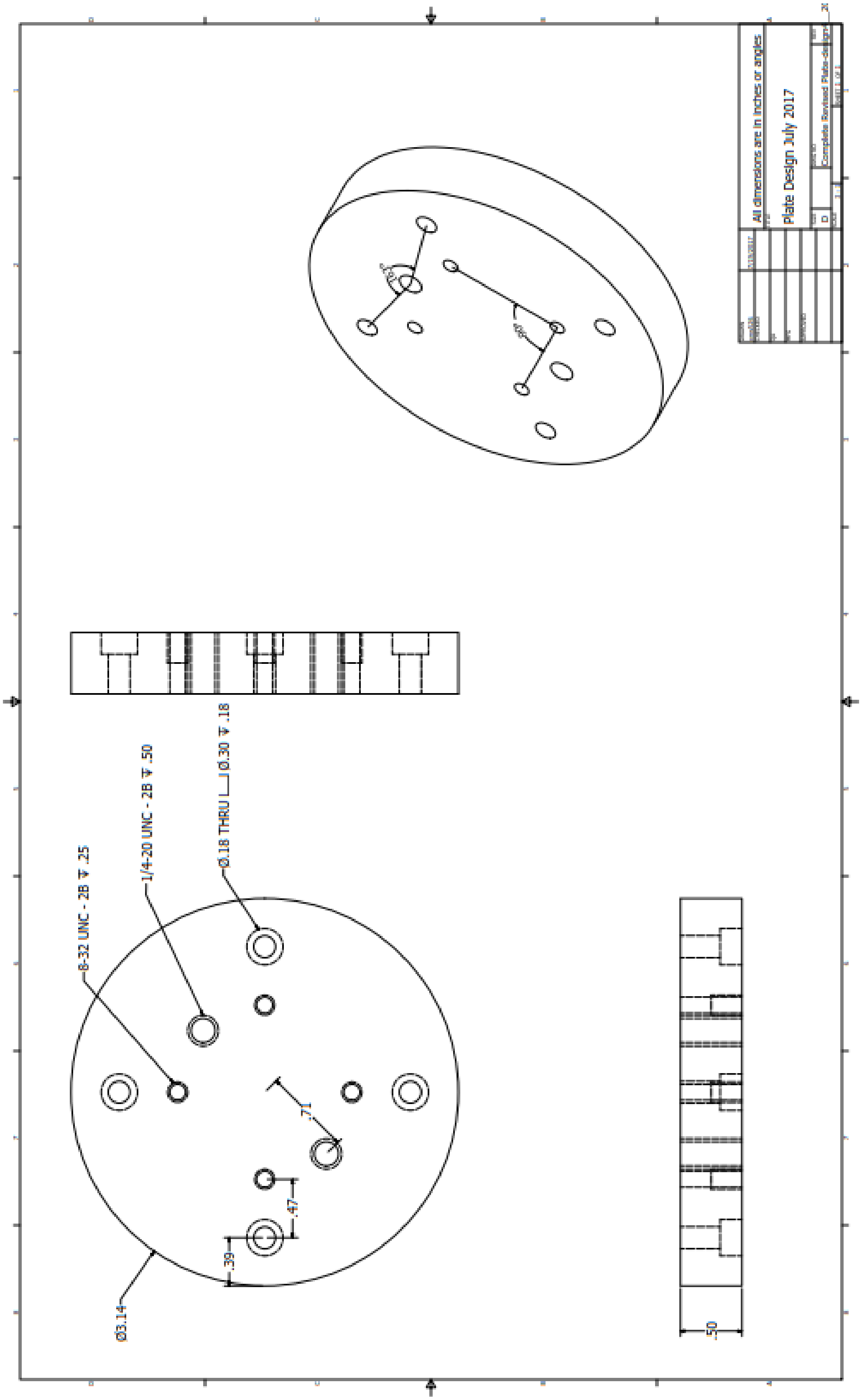

Appendix Figure 3: Detailed drawings of the binding plate